ON THE LACK OF CATASTROPHIC COLLSIONS IN THE PRESENT KUIPER BELT. Abedin. Y. Abedin[1] and JJ. Kavelaars[1], [1]Herzberg Astronomy and Astrophysics, National Research Council Canada, 5071 West Saanich Road, Victoria V9E 2E7, Canada.

Introduction: The size-frequency distribution (SFD) of trans-Neptunian objects (TNOs) informs about their past collisional evolution i.e., whether their SFD is a result of collisional equilibrium or it reflects the primordial planetesimal accretion stage. Previous studies, indicate that collisions have played an important role in shaping the SFD of TNOs e.g., [1-5]. However, recent "streaming instability" (SI) simulations, of the planetesimal growth, indicate that the cumulative SFD of TNOs (r < 50 km), does not necessarily imply collisional equilibrium but could be also explained as a natural outcome the model [6,7,8].

In this work, we explore several cases, with different TNO SFDs and initial population estimates (P.E.), to test whether catastrophic collisions have been important in the present Kuiper belt, since the giant planets established their current orbits. This would help us better understand the collisional environment beyond Neptune's orbit and also test the hypothesis for *in-situ* formation of the cold classical Kuiper belt objects (CCKBOs). The low number of craters on the CCKBO "Arrokoth" [9], as measured by the NASA New Horizons mission, has already put constraints on the planetesimal number density, between 42-47 AU, and their collisional evolution.

The size-frequency and orbital distribution of TNOs: We utilize the orbital and size-frequency distributions of TNOs, based on the debiased ensemble sample of the Outer Solar System Origins Survey (OSSOS++) [10-14]. Figure 1 shows a schematic of TNO absolute magnitude H_r - distribution, adopt in this work and used to convert H_r to radius. The $H_r \mapsto R$ conversion is done by assuming a geometric albedo of 14% and 8% for the *cold* and excited (*Resonant*, *Hot, Detached+Outer belt* and *Scattering objects*) TNO populations, respectively.

We also assume that the orbital structure of the present Kuiper belt has not changed much, since the TNOs have been emplaced into their current heliocentric orbits. We consider five dynamically distinct TNO orbital classes (the *Resonant*, *Cold*, *Hot, Detached+Outer belt* and *Scattering objects*), based on the nomenclature described in [15]. We further, arbitrarily, divide the resonant TNOs into three subgroups (*inner, main* and *outer* resonant objects). These three resonant sub-populations are, in terms of increasing semi-major axis, inner resonant (4:3 and 3:2), main resonant (5:3 and 7:4) and outer resonant (2:1, 7:3 and 5:2) objects. This provides a better resolution in testing which of these resonant sub-populations are more likely to experience collisions, over some time T.

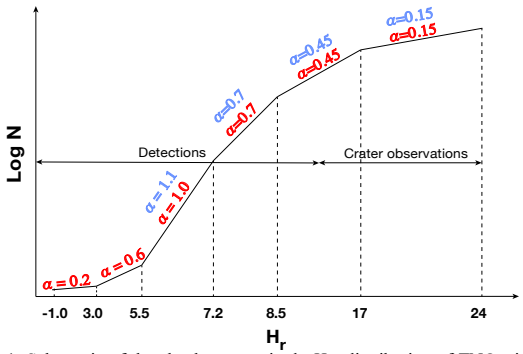

Fig 1. Schematic of the absolute magnitude H_r - distribution of TNOs, in the r-band, based on the OSSOS++ ensemble sample. The color labels refer to the logarithmic slopes of the cold (blue) and excited (red) TNO populations, respectively. The horizontal lines indicate the approximate H_r extent of ground and space-based TNO observations and the ones derived from crater SFD on Pluto-Charon system [16] and the CCKBO Arrokoth [9], by the New Horizons mission.

Modelling the collisions in the present Kuiper belt, under different TNO SFD cases: Using the OSSOS++ orbital distribution of TNOs, [17] calculated the intrinsic collision probabilities (ICPs) within and between different TNO dynamical populations. Based on that and the OSSOS++ TNO SFD, we then calculate the radius "r", of the largest impactor, from a given TNO population, that can collide with a single target of radius "R", belonging to another TNO population, over some time T. We thus have a set of functions $\boldsymbol{r} = \boldsymbol{r}\,(R, T)$, where $\boldsymbol{r} = \{r_{\rm cold}, r_{\rm hot}, r_{\rm inres}, r_{\rm mainres}, r_{\rm outres}, r_{\rm detached+outer}, r_{\rm scattering}\}$, where the subscript refers to the impactor population. From that we obtain an average $\bar{r}$, where the latter is weighted by the relative P.E. of each TNO component. In a similar way, we calculate a spectral distribution for the specific impact energy $\overline{\boldsymbol{Q}}_S = \overline{\boldsymbol{Q}}_S(R,T)$ between impactors of $\boldsymbol{r} = \{r_{\rm cold}, r_{\rm hot}, r_{\rm inres}, r_{\rm mainres}, r_{\rm outres}, r_{\rm detached+outer}, r_{\rm scattering}\}$ and a single target of radius R, belonging to a given TNO population. In the latter calculation, we assume a uniform impact speed of v =3 km/s and equal impactor-target bulk density of ρ=500 kg/m^3. Our choice of a uniform impact speed of v =3 km/s is motivated from the calculated ICPs and impact speeds [17,18], between different TNO populations, where "v" is very unlikely to exceed even ~2 km/s. Thus, our assumed impact speed of v =3 km/s serves as an upper limit of the specific impact energies $\overline{\boldsymbol{Q}}_S$. The calculated $\overline{\boldsymbol{Q}}_S$=$\overline{\boldsymbol{Q}}_S(R,T)$ are then compared to the

catastrophic disruption threshold values $\boldsymbol{Q_D^\star}$=$\boldsymbol{Q_D^\star}(R, r, \rho_t, \rho_i, v)$, based on "Smooth-Particle-Hydrodynamic" (SPH) simulations by [19] and [20], relevant for icy bodies, colliding with speeds v=0.5 km/s and v=3 km/s. The above calculations are then perform ed for six different cases - {"nominal", "case_x200_4 GYR", "case_x500_300MYR", "case_x2000_300MY R", "case_H85_06_4GYR" and "case H85_07_300M YR}. The nominal case assumes the P.E. values of TNOs, at H_r=8.5, presented in [17] and the SFD in Fig.1, and collisions considered over 4 Gyr. In the next three cases, the name format used is: "case_X,_Y"; where X= the P.E. of TNOs at H_r=8.5, relative to the nominal case" and Y= the time interval, over which collisions have been considered. In the last two cases, H85_X= the adopted value of the logarithmic slope α, for 8.5 < H_r < 17, where Y is as before. The last two cases, essentially explore the scenario of the number of objects between 8.5 < H_r < 17 was higher.

Results: Figure 2 shows the average specific impact energies $\overline{\boldsymbol{Q}}_s$, between an impactor and a single target of radius R, belonging to the CCKBOs. It is evident that given the current orbital and SFD architecture of the Kuiper belt, and assuming it did not change much over the last 4 Gyr, the average specific impact energies $\overline{\boldsymbol{Q}}_s$, from the largest impactors are well below the catastrophic disruption threshold $\boldsymbol{Q_D^\star}$, according to the SPH simulation results of [19] and [20] for collisions with 0.5 km/s and 3 km/s. An alternative way of showing our results is to consider the average number of catastrophic collisions N_C, a CCKBO target of radius R has experienced over time (Fig. 3). Thus, based on the current TNO orbits, the only cases in which collisions could initiate catastrophic disruptions and cascading fragmentation are: "Case_x200_4GYR" and "Case_x2000_300MYR". The first case requires an early Kuiper belt mass of 200 times the current estimates (0.01-0.02 $M_\oplus$) [21] and collisions to have lasted for 4 Gyr. The second case could trigger catastrophic collisions within only 300 Myr, after planetesimal emplacement into their current orbits, given the mass of the young Kuiper belt was 20 $M_\oplus$< M < 40 $M_\oplus$. Both cases imply that the CCKBOs with $R \gtrsim$ 50 km have never experienced catastrophic collisions and hence their SFD must reflect the primordial planetesimal accretional stage. Smaller objects, on the other hand, must be collisionally derived fragments. According to our study, only ~3% of the CCKBO would have experienced catastrophic collisions under our nominal case (Fig. 3), while the remaining cases result in a significant collisional erosion. However, the presence of weakly-bound binaries among the CCKBOs [22, 23, 24] puts a solid constraint on the collisional environment in that region, beyond Neptune's orbit. It is difficult to reconcile the relatively large fraction (< 30 %) of binary CCKBOs and the catastrophic disruptions under the remaining cases. Likely, the CCKBOs formed *in situ*, in a low collisional environment, and their SFD reflects the primordial planetesimal accretion stage.

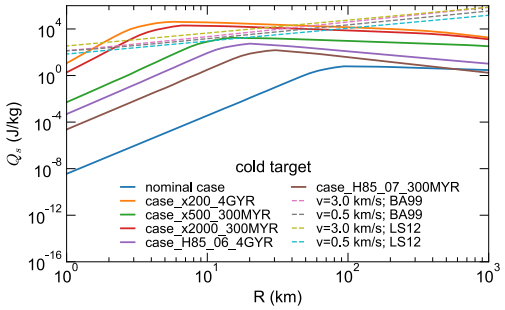

Fig 2. Average specific impact energy $\overline{\boldsymbol{Q}}_s$, weighted by the relative P.E., at H_r = 8.5, between impactors from all TNO populations, as a function of target radius R, belonging to the CCKBOs. Each color line denotes different case explained in the text. The color dashed lines correspond to the catastrophic disruption thresholds for icy targets of radius R, colliding with speeds 0.5 and 3 km/s, based on SPH simulations by [19] and [20].

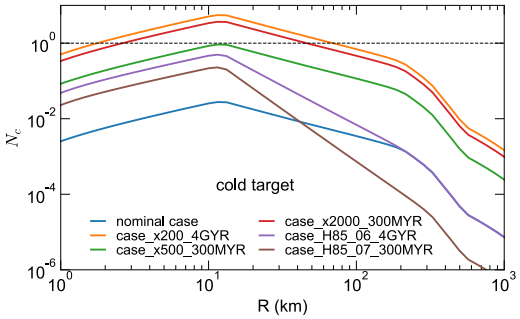

Fig 3. Average number of catastrophic collisions N_c, as a function of target radius R, belonging to the CCKBO population. The weighting of N_c has been performed as in Fig.2. Each color line denotes N_c under different cases explained in the text. The black dashed line marks the location where N_c=1.

References: [1] Stern, S. A. (1995) AJ. 110, 856; [2] Stern, S. A (1996) AJ. 112, 1203; [3] Farinella, P. and Davis, D. R. (1996) Sci. 273, 938; [4] Kenyon, S. J. and Bromley, B. C. (2017) ApJ. 839, 38; [5] Kenyon, S. J. and Bromley, B. C. (2020) PSJ. 1, 40; [6] Youdin, A. N., Goodman, J. (2005) AJ. 620, 459-469; [7] Abod C. P. et al. (2019) AJ. 883, 192; [8] Kavelaars JJ. et al. (2021) AJL. 920:L28; [9] Spencer, J. et al. (2020) Sci. 367, 6481; [10] Kavelaars , JJ et al. (2009) AJ, 137,6; [11] Petit, J.M. et al. (2011) AJ. 142, 4; [12] Alexandarsen M. et al (2016) AJ. 152, 5. [13] Bannister, M. et al (2018) ApJS. 236,1.; [14] Lawler, S. et al. (2018) AJ 155, 5.; [15] Gladman, B. ; Marsden, B. G. ; Vanlaerhoven, C. (2008) SSBN p.43-57; [16] Singer, K. et al. (2016) Sci. 363, 6430; [17] Abedin, A. et al. (2021) AJ. 161, 195A; [18] Greenstreet, S. et al. (2015) Icar. 258, p. 267; [19] Benz, W.and Asphaug, E. (1999) Icar. 142, 1; [20] Leinhardt, Z. and Stewart, S. (2012) ApJ 745, 1; [21] Pitjeva, E. V. and Pitjev, N. P. (2018) CeMDA 130, 57; [22] Noll, K. C. et al. (2008) SSBN p. 345; [23] Grundy, W. et al. (2011) Icar., 213, 2, p. 678 [24]; Fraser, W. et al. (2017) Nat. Ast. Vol.1; [25] Fraser, W. et al. (2021) PSJ. 2, 3, 90.